High Reynolds Number Flow in Capillary Tube with Spiral/Bend Portion (Experimental Results for Water)

High Reynolds Number Flow in Capillary Tube with Spiral/Bend Portion

(Experimental Results for Water)

Kazuo MAENO, Akihiro YAMAZAKI and Yutaka HANAOKA

Abstract

Experimental study on water flow in capillary tubes with straight, bent, or coiled portion is conducted. Stainless tubes with nominal diameter of 0.5mm, 0.25mm, and 0.1mm are examined at several temperatures. Reynolds number ranges from 30 to 16000, where maximum velocity becomes up to 30m/s. Pressure loss of test piece and discharge flow rate are measured to be compared with the results from previous studies. In spite of considerable roughnesses of capillary inner surface, measured data do not indicate roughness effect explicitly. Laminar friction factors for coiled tubes show the clear dependence on the number of turns in the coil, which cannot be explained by previous studies. Empirical equations for examined capillary contours are obtained.

NOMENCLATURE

A : Tube cross sectional area
a : Tube inner radius
D : Tube inner diameter
g : Gravitational acceleration
H : Total head loss
ΔH_a : Head loss in entrance region
$\Delta H'$: Head loss in recovery region
Δh : Head loss in curved portion
K_l : Dean number $[=R_e(a/R)^{1/2}]$
K_t : Turbulent characteristic number $[=R_e(a/R)^2]$
k_s : Roughness
L : Tube length
L_a : Length of entrance region
l : Length of curved axis
N : Number of turns in the coil
p : Pressure difference between both sides of tube
Q : Weight flow rate
R : Radius of curvature at curved tube axis
Re : Reynolds number

T : Water temperature
v : Average velocity
v_* : Friction velocity
α : Coefficient (Eq. 16)
ε : Relative roughness
ζ : Loss coefficient in curved tube
θ : Turning angle of curved tube
λ : Friction factor
ν : Kinematic viscosity
ξ : Loss coefficient of entrance region
ρ : Density

Subscript and Superscript

a : Entrance
b : Bend tube
c : Coil
s : Straight tube
l : Laminar
t : Turbulent

1. INTRODUCTION

The behavior of flow in pipes and ducts has been the important objective of many fluid dynamical reseraches.[1),2)] Especially for the flow in curved tubes, problems of friction losses and flow pattern have been extensively investigated since the 1920's.[3),4),5)] In curved tubes originated is the secondary circulating flow in the plane containing the line of curvature center by centrifugal force difference between the inward flow and outer flow region adjacent to the wall. With these secondary spiral pair flows, pipe frictional loss shows the greater value than in the straight tube. According to the results of previous studies, the friction factor λ_c of curved tube can be specified by Dean number $K_l=R_e\,(a/R)^{1/2}$ in laminar flow region and by characteristic number $K_t=R_e\,(a/R)^2$ when the flow is turbulent.

These systematical investigations, however, have been restricted to relatively large tube diameters ($D\geqq$1mm). Except for the capillary tube flow of low Reynolds number in viscosity measurement or in bioengineering study, neither experimental nor analytical researches has been adequate for the flow in tubes with small diameter ($D<$1mm).

In connection to the space technology, curved capillary tube is commonly utilized as propellant feed tube[6)] of hydrazine thruster[7)] for attitude control equipped to spacecrafts, satellites in geosynchronous orbit, and so forth. Propellant (liquid hydrazine) is fed through this capillary tube to thermal and catalytic decomposition chamber by high-pressurized N_2 gas. This tube is contrived to shield from high-temperature effect of chamber, and to stabilize the feed conditions of N_2 blowdown in restricted room.

In this paper an experimental investigation on water flow in capillary tube is con-

ducted, as the fluid dynamical properties of water resemble to those of hydrazine. Stainless tubes (SUS 304) with nominal diamerer of 0.5mm, 0.25mm, and 0.1mm are employed, and Reynolds number ranges from 30 to 16000. Each tube is re-formed to straight, bend, coil or combined shaped test piece for the measurement of pressure loss and discharged flow rate. Measured data are compared with the results for tube of usual diameter.[1),2)] The maximum water temperature of the measured data is 60°C.

2. MEASUREMENTS

2-1. Hydrazine and Water

For the thruster of gas jet type, which is utilized to control the attitude of station-keeping satellite, hydrazine and its combinations are usually employed as propellant. Table 1 shows the properties of hydrazine, its combinations, and water. In Tables 2 and

Table 1 Properties of Hydrazine and Water

Fluids	Hydrazine	Hydrazine Hydrate	Unsym.-Dimethyl Hydrazine	Monomethyl Hydrazine	Water
Chemical Formula	N_2H_4	$N_2H_4.H_2O$	$(CH_3)_2N_2H_2$	$CH_3N_2H_3$	H_2O
Melting Point [K]	274.69	233.2	215.96	220.76	273.16
Boiling Point [K]	386.66	391.7	336.26	360.66	373.16
Heat of Vaporization [kcal/mol]	10.70	10	8.336	9.468	9.719
Heat of Fusion [kcal/mol]	3.025	-------	2.407	2.491	1.436
Density [g/cm^3] (K)	1.017(283.16) 1.004(298.16)	1.03(294.16)	0.784(298.16)	0.874(298.16)	0.998(293.16)
Heat of Formation (25℃) [kcal/mol]	+12.05	−10.3	+11.3	+13.1	−57.798 (Vapor)
Specific Heat [kcal/kg.℃]	0.75(300.16)	-------	0.638(273.16) 0.652(298.16)	0.699(293.16)	0.998(293.16) 0.997(300.16)
Viscosity Coefficient [cp] (K)	1.29(274.16) 1.12(283.16) 0.97(293.16)	3.5(273.16) 2.0(293.16)	1.7(243.16) 0.78(273.16) 0.51(298.16)	0.893(298.16)	1.792(273.16) 1.002(293.16) 0.892(298.16)
Thermal Conductivity [kcal/m.h.℃]	0.18(300.16)	-------	0.1785(298.16)	-----	0.500(283.16) 0.522(300.16) 0.571(340.16)
Surface Tension [dyn/cm] (K)	91.5(298.16)	-------	-----	-----	72.61(294.16) 71.96(298.16) 71.15(300.16)
Vapor Pressure [mmHg] (K)	76(327.16) 2280(422.16)	-------	41(273.16) 450(323.16)	49.6(298.16) 17.1(323.16)	17.5(293.16) 92.5(323.16)

Table 2 Viscosity and density of hydrazine vs. temperature

Temp.[℃]	Viscosity [cp]	Density[g/cm³]
0	1.314	1.0258(0℃)
5	1.207	
10	1.118	
15	1.044	
20	0.974	1.0085(20℃)
25	0.905	
37.8	0.743	0.980 (50℃)
93.3	0.417	

Table 4 Solubility of N_2 into water

Temperature [℃]	Pressure [atm]	Solubility [molar fraction]
51.5	1	$0.0894(\times10^{-4})$
	100	$7.99(\times10^{-4})$
	200	14.54
	300	20.17
102.5	1	$0.0797(\times10^{-4})$ [100℃]
	101	7.77
	201	14.47
	302	20.05

(1 atm = 760mmHg = 1.033kgf/cm²)

Table 3 Temperature and pressure dependence of H_2O properties

Temp. [℃]	Pressure [kgf/cm²]	Specific Weight [kgf/m³]	Viscosity [kgf. s/m²]	Kinematic Viscosity [m²/s]
0	1	999.9	$182.9(\times10^{-6})$	$1.794(\times10^{-6})$
	500	1023.5	171.6	1.644
	1000	1044.9	168.5	1.581
30	1	995.7	$81.6(\times10^{-6})$	$0.8028(\times10^{-6})$
	500	1017.3	83.6	0.8059
	1000	1036.3	85.9	0.8129
75	1	974.6	$38.9(\times10^{-6})$	$0.3909(\times10^{-6})$
	500	996.0	40.2	0.3958
	1000	1014.2	41.8	0.4042

3 presented are the temperature dependence of viscosity and other properties. It can be noticed from these tables that the fluid dynamical properties of hydrazine are closely akin to those of water, e.g. at 293K hydrazine density is almost 1% greater and its viscosity has less value of about 3% than water. The experimental results for water, therefore, can be applied to the presumption of characteristics of hydrazine tube flow, provided that hydrazine remains in single liquid phase. The solubility of nitrogen in water seems to be negligible as indicated in Table 4, so, its influence is not taken into account.

2-2. Capillary Tube

The microscopic photographs of cross section of capillary tubes are shown in Fig. 1. Being rasped off the outer surface, tube is snapped to be filed its edge cross section by sandpapers of No. 600-1500. It can be seen from these photographs that capillary tubes have considerable roughness on their inner surfaces. With measuring the size of these cross sections, average diameters in Fig. 1 can be estimated, which have the coincidence with equivalent hydraulic diameters obtained by straight tube experiments in laminar region. Based on these average diameters, relative roughnesses of 0.55mm, 0.29mm, and

0.115mm tube can be determined to be about 2.5%, 4%, and 7.8%.

The influence of bending and coiling on tube inner diameter is also examined by cross sectional photographs of bent tube. In our measurements, no appreciable deformation of cross sectional shape is observed.

2-3. Experimental Apparatus

Schematic diagram of experimental setup is represented in Fig. 2. Water is supplied from hydrant through a coarse filter into the pressure vessel. The vessel is heated by band heater 1 for water preheating, and N_2 gas from regulator pressurizes the water to assigned range. Pressurized water is further heated up to the adjusted temperature by heater 2. Then it passes from valve 3 through the portion of hot water heat insulation, and filtrated by teflon filter (NRK Uniflon Filter FZ-B, 3-5μm) before going into the test piece tube. Main piping before the test piece is nylon tube (Nitta-Moore Nylon Tubing, Max. 70 kgf/cm^2). The pressure in the vessel is monitored by Bourdon's gauge 1 (Nagano, 0-25 kgf/cm^2, 0.5 class), and water pressure upstream of test piece is also measured by gauge 2 (0.5 class for high pressure range and 1.5 class for low range), together with the temperature measurement by C-A thermocouple and digital multimeter. The discharged water from test tube is received by beaker to be weighed its flow rate by the balance of scales (Murayama, VS-10, F.S. 2010g, 1/20000).

Tube test pieces are fabricated in the following process. Stainless capillary is cut and adjusted its end surface by fine sandpapers from No. 600 to No. 1500. Then it is

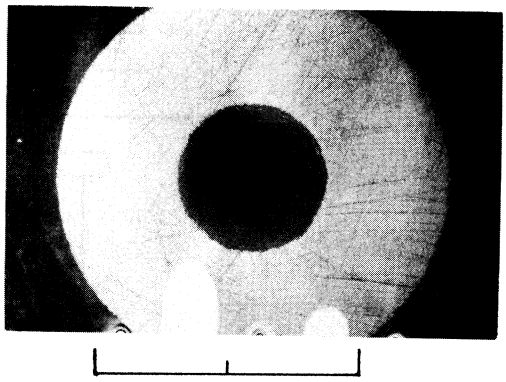

Fig. 1 Microscopic photographs of capillary tube cross section

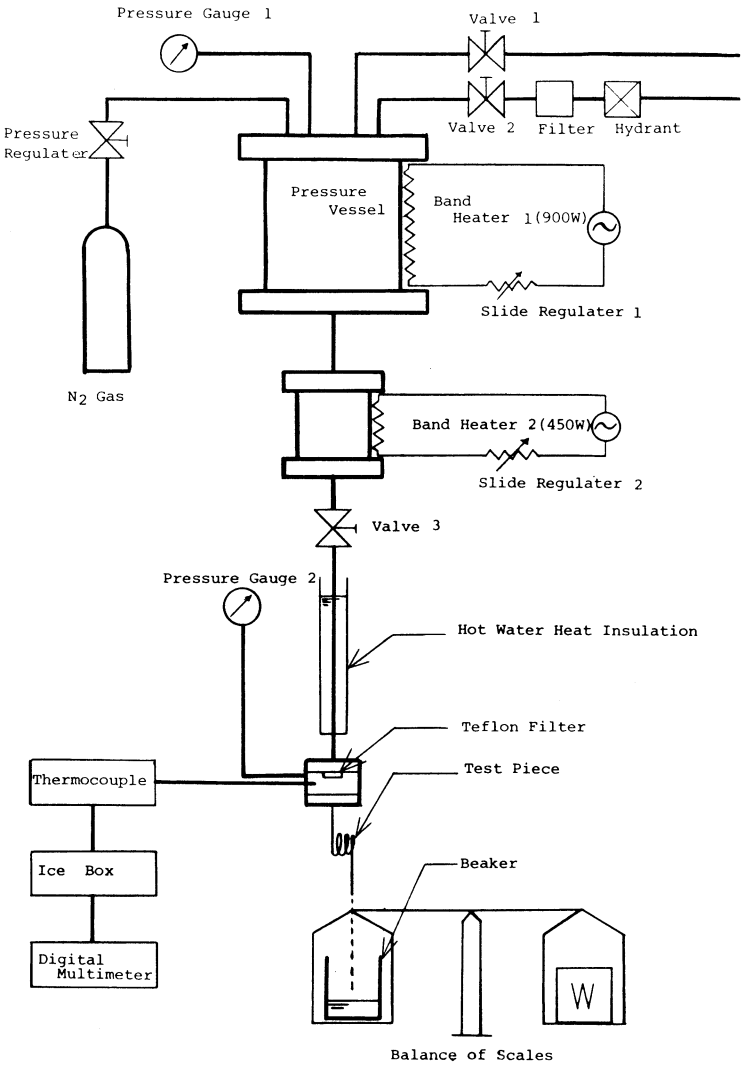

Fig. 2 Schematic diagram of experimental apparatus

equipped with Araldite to tube adapter and measured its length by vernier caliper or scale. Inner surface of test piece is cleaned by usual stainless steel cleaner. And the straight tube is re-formed to have bent or coiled portion with the curvature measured by R-gauge. Figure 3 shows the contour of bent/coiled tubes, and their photographs are presented in Fig. 4. The specifications of typical tubes tested are indicated in Table 5.

2-4. Analysis of Tube Flow Data

In our analysis of measured data, well-known relations for pipe flow can be applied ;

$$Q=\rho g A v, \tag{1}$$

$$Re=\frac{vD}{\nu} \tag{2}$$

$$H=\lambda\frac{L}{D}\frac{v^2}{2g},$$

〔Darcy-Weisbach's Equation〕 (3)

Laminar ; $\lambda^l=\frac{64}{\mathrm{Re}}$,

〔Hagen-Poiseuille〕 (4)

Turbulent; $\lambda^t=0.3164/Re^{1/4}$,

〔Blasius〕. (5)

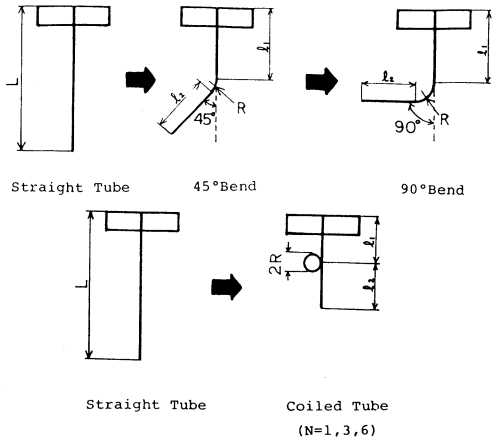

Fig. 3 Capillary tube contours

Table 5 Dimension of typical tubes tested

(a) Straight Tube

D	L	D	L
0.55	52.2	0.29	50.3
0.55	100.4	0.29	99.8
0.55	150.1	0.29	149.0
0.55	199.5	0.29	201.2
0.55	249.8	0.29	250.1
0.55	299.0	0.29	302.3
0.55	507.0	0.29	498.3
0.115	49.2		
0.115	82.1		
0.115	204.8		

(b) 45° Bend

D	L	R	l_1	l_2
0.55	299.0	5.0	146.0	149.0
0.29	302.3	5.0	142.0	156.4

(c) 90° Bend

D	L	R	l_1	l_2
0.55	299.0	5.0	144.0	147.0
0.29	302.3	5.0	139.5	155.0
0.29	302.3	9.5	151.5	135.9

(d) Coiled Tube

D	L	R	l_1	l_2	N	θ	P
0.55	507.0	10.5	79.0	362.0	1	360	3.4
0.55	507.0	10.5	79.0	230.0	3	1080	3.4
0.55	507.0	10.5	79.0	32.2	6	2160	3.4
0.29	498.3	9.9	63.1	373.0	1	360	4.2
0.29	498.3	9.9	63.1	248.6	3	1080	4.2
0.29	498.3	9.9	63.1	62.0	6	2160	4.2
0.29	498.3	6.2	93.1	366.2	1	360	2.6
0.29	498.3	6.2	93.1	288.3	3	1080	2.6
0.29	498.3	6.2	93.1	171.5	6	2160	2.6
0.115	82.1	5.9	38.3	6.7	1	360	1.3

D: Inner Diameter [mm] N: Number of Windings θ: Turning Angle [deg.]
P: Coil Pitch [mm]

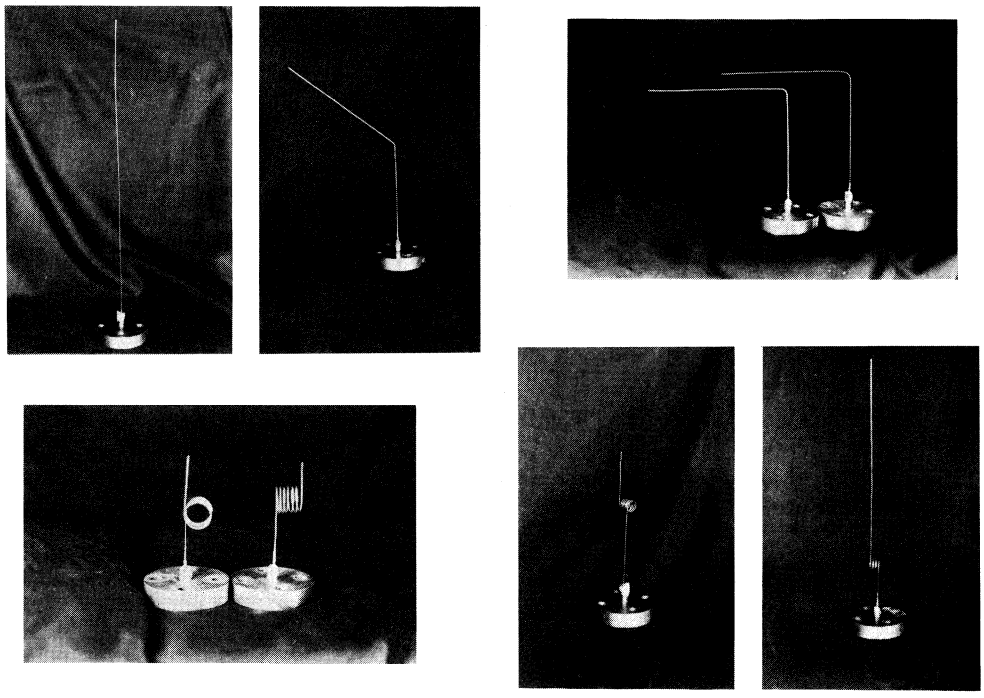

Fig. 4 Photographs of capillary tubes

In capillary experiments direct measurement of velocity distribution is almost impossible without visualization by transparent tube materials. So the results of measurement also require us to have consideration of the length and loss of developing flow in entrance region.

For entrance length L_a of straight capillary, equation from McComas[8] in laminar range as ;

$$L_a^l = 0.0260 \cdot R_e \cdot D, \qquad \text{[entrance loss coefficient ; } \xi = 1.33\text{]} \tag{6}$$

and analytical relation by Bowlus and Brighton[9] for turbulent flow as ;

$$L_a^t = (14.25 \log Re - 46.0)D \tag{7}$$

are taken. In addition to these relations, velocity distribution is roughly assumed to be the same as those in laminar Hagen-Poiseuille flow or turbulent 1/7 power law.

The hydraulic head can be expressed in the following manner ;

$$H = \Delta H_a + \lambda_s \frac{L - L_a}{D} \frac{v^2}{2g}, \tag{8}$$

and head loss in the entrance region is given by

$$\Delta H_a=(\lambda\frac{L_a}{D}+1+\xi)\frac{v^2}{2g}. \tag{9}$$

From these equations friction factor for straight tube can be obtained as follows ;

〔Laminar〕

$$\lambda_s^t=\frac{D}{L-0.0260\ Re\ D}\left(\frac{2gH}{v^2}-64\times0.0260-1-\xi\right), \tag{10}$$

$$\xi=1.33,$$

〔Turbulent〕

$$\lambda_s^t=\frac{D}{L-(14.25\log Re-46.0)\ D}\left\{\frac{2gH}{v^2}-\frac{0.3164}{Re^{1/4}}(14.25\log Re-46.0)\right\}, \tag{11}$$

$$\xi=0.06.$$

As regards the curved tube with straight portion, along with the same procedure above applied, recovery length and loss must be considered. Though exact estimation is impossible, because of the lack of velocity distribution data, it may be roughly approximated that the length is equal to entrance length L_a and recovery loss $\Delta H'$ is the friction loss of developed flow (almost no effect). To our regret, the effects of velocity distribution change are neglected.

According to these considerations, total head loss Δh in purely curved region is given as ;

$$\begin{aligned}\Delta h&=H-\Delta H_a-\Delta H'-\lambda_s\frac{L-2L_a-l}{D}\frac{v^2}{2g}\\&=H-(\lambda\frac{L_a}{D}+1+\xi)\frac{v^2}{2g}-\lambda\frac{L_a}{D}\frac{v^2}{2g}-\lambda_s\frac{L-2L_a-l}{D}\frac{v^2}{2g},\end{aligned} \tag{12}$$

$$l=\frac{\pi R\theta}{180}. \tag{13}$$

Loss coefficient ζ and friction factor λ_c (λ_b) are ;

$$\zeta=\frac{\Delta h}{\left(\frac{v^2}{2g}\right)}, \tag{14}$$

$$\Delta h=\lambda_{c(b)}\frac{l}{D}\frac{v^2}{2g}. \tag{15}$$

Measured data are analyzed by off-line computer (SORD M-23).

With respect to the turbulent flow in bend tubes of smooth inner surface and circular cross section, empirical equations of total loss coefficient by Itō[5] are reported ;

for $R_e\left(\frac{a}{R}\right)^2<91$,

$$\zeta=0.00873\alpha\lambda_c\theta\frac{\mathrm{R}}{\mathrm{a}}, \tag{16}$$

and for $Re\,(\frac{a}{R})^2 > 91$,

$$\xi = 0.00241\ \alpha\theta Re^{-0.17}\,(\frac{R}{a})^{0.84} \tag{17}$$

where the coefficient α is given as follows ;

〔45° bend〕 $\alpha = 1 + 14.2\,(\frac{R}{a})^{-1.47}$,

〔90° bend〕 $\alpha = 0.95 + 17.2\,(\frac{R}{a})^{-1.96}$, $\quad(\frac{R}{a} < 19.7)$

$\alpha = 1$, $\quad(\frac{R}{a} > 19.7)$

$(\frac{R}{a} > 2,\ 2\times10^4 < Re < 4\times10^5)$.

As regarding the curved tube, systematical researches by Itō[10),11),12)] have offered the following equations ;

For laminar range,[10),11)]

$$\frac{\lambda_c}{\lambda_s} = \frac{21.5\,K_l}{(1.56 + logK_l)^{5.73}}, \qquad (13.5 < K_l < 2\times10^3)\ , \tag{18}$$

or

$$\frac{\lambda_c}{\lambda_s} = 0.1008 K_l^{1/2}\,(1 + 3.945 K_l^{-1/2} + 7.782\,K_l^{-1} + \cdots\cdots), \quad (K_l > 30)\ . \tag{19}$$

For turbulent range,[12)]

$$\lambda_c\,(\frac{R}{a})^{1/2} = 0.029 + 0.304\ \{Re\,(\frac{a}{R})^2\}^{-1/4} \quad (0.034 < Re\,(\frac{a}{R})^2 < 300)\ . \tag{20}$$

Taking account of Equations (16)-(20), our arrangement of measured data is concentrated to find linear relations in logarithmic coordinates between $\lambda_c\,(R/a)^{1/2}$ and Dean number for laminar flow, or characteristic number $Re\,(a/R)^2$ for turbulent flow.

3. RESULTS AND DISCUSSION

3-1. Straight Capillary Tube

As preliminary experiments, straight capillaries of different length were examined at room temperature. Figure 5 - (a), (b), (c) show the discharged characteristics. With these results, calculated frictional resistance factors are indicated in Fig. 6 - (a), (b), (c), (d), (e). Friction factors for tubes with 0.55mm diameter indicated in Fig. 6 - (a), (b) show good agreement in laminar region with theory, while somewhat smaller distributions than Blasius' relation in turbulent flow are obtained, which can not be explained enough. Reynolds number ranges up to 16000 where average velocity in capillary becomes about 30m/s and passage duration of water in tube is the order of millisecond. For 0.29mm tubes in Fig. 6 - (c), (d) the transition point from laminar to turbulence shifts to higher Reynolds number range as the tube length becomes shorter. This tendency may concern with the

entrance length estimation. As regards 0.115mm tubes, only laminar data are obtained as shown in Fig. 6 - (e). It can be seen from Fig. 6 that the hydraulic diameters obtained from microscopic photographs correspond approximately with the results in laminar region.

In connection with temperature dependency of flow characteristics, measured distributions of friction factor for 0.55mm tube are indicated with diverse temperatures in Fig. 7 - (a), (b). From these figures it is recognized that temperature increment results in the extension of Reynolds number to higher range, as kinematic viscosity decreases.

It is well known that in turbulent region roughness of tube surface affects the friction factor. From the measurements described in section 2-2, considerably large relative roughness of 2.5% is observed even in 0.55mm tube, where the strong influence can be surmized as in the Moody plot. In general, for fluid dynamically smooth pipe following relation is given ;

$$\frac{1}{\sqrt{\lambda}}-2\log\left(\frac{a}{k_s}\right)=2\log\left(\frac{k_s v_*}{\nu}\right)+0.705, \quad \left[\frac{k_s v_*}{\nu}\leqq 5\right], \tag{21}$$

and fluid dynamically rough tube shows ;

$$\frac{1}{\sqrt{\lambda}}-2\log\left(\frac{a}{k_s}\right)=1.74, \quad \left[\frac{k_s v_*}{\nu}\geqq 70\right]. \tag{22}$$

In the transient range, Colebrook's relation is formed ;

$$\frac{1}{\sqrt{\lambda}}=-2\log\left(\frac{\varepsilon}{3.7}+\frac{2.51}{Re\sqrt{\lambda}}\right).$$

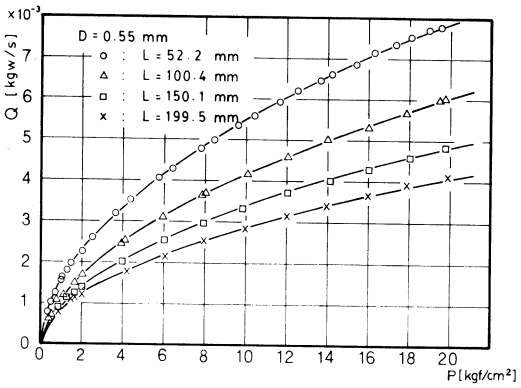

(a)

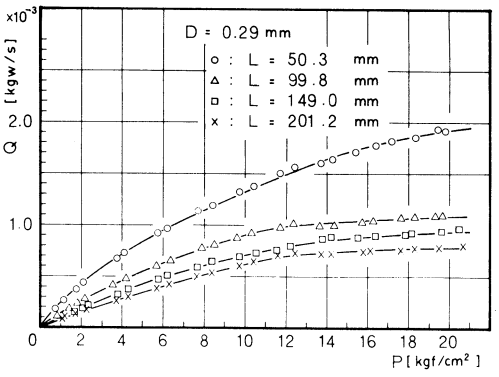

(b)

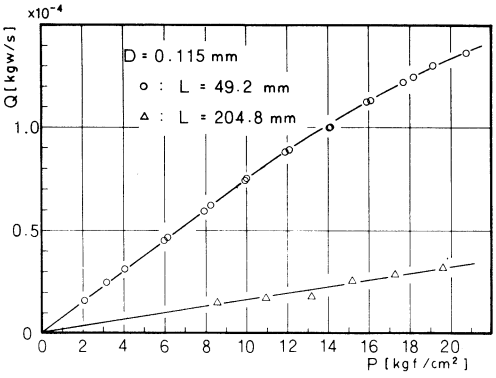

(c)

Fig. 5 Discharged flow rate versus gauge pressure (water of room temperature)

$$\left[5 \leqq \frac{v_* k_s}{\nu} \leqq 70\right]. \tag{23}$$

It is impossible to obtain the velocity distribution in our capillary, so friction velocity of the measurement is calculated by

$$\frac{v_*}{v} = \sqrt{\frac{\lambda}{8}}, \tag{24}$$

where directly measured friction factor λ is utilized.

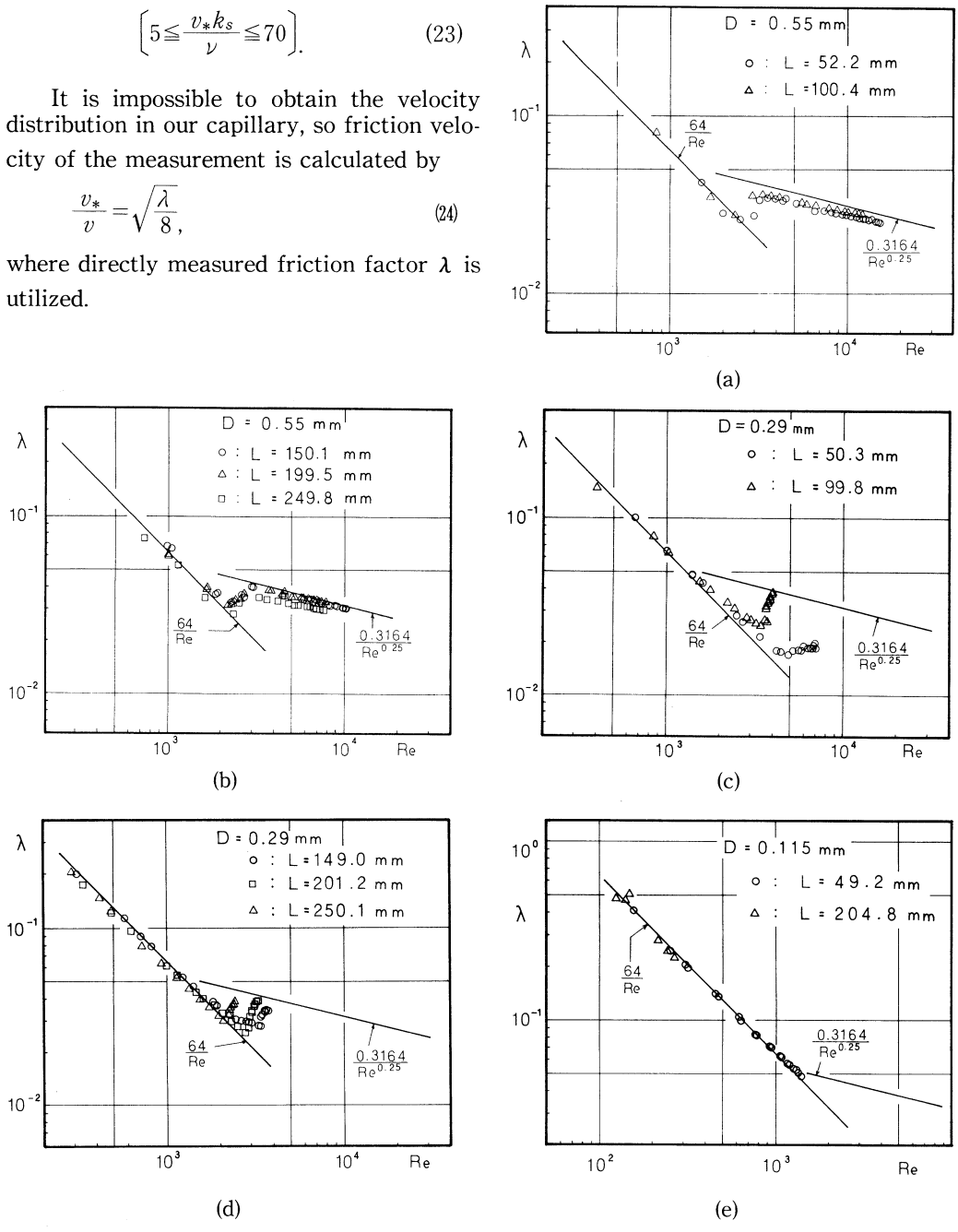

Fig. 6 Frictional resistance factor for straight tube (water of room temperature)

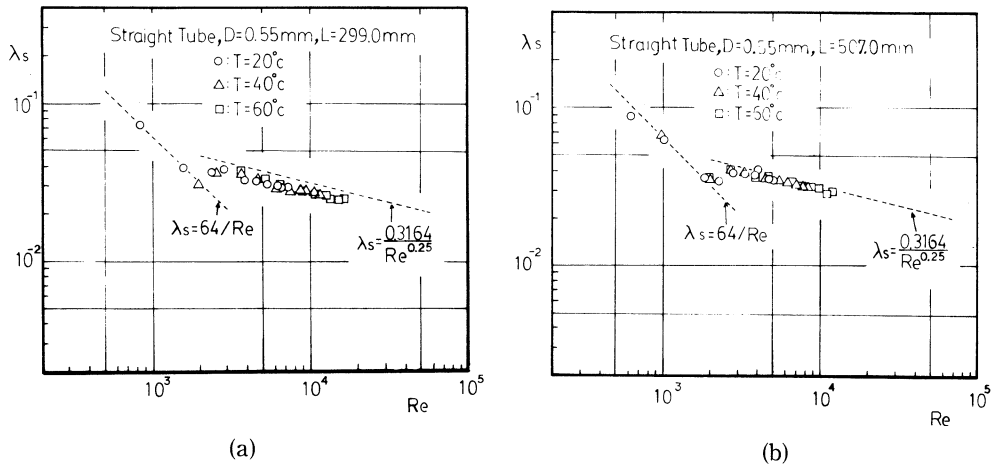

(a) (b)

Fig. 7 Frictional resistance factor for 0.55mm tube (with varying water temperature)

Figure 8 indicates the effect of fluid dynamical roughness for 0.55mm tubes in Fig. 7. Different from usual tubes, measured results present no transition to fluid dynamical rough curve even in the region where

$$\log\left(\frac{k_s v_*}{\nu}\right) \cong 1.4.$$

It can be remarked from this figure that in capillary tube the roughness effect of inner furface does not appear explicitly, and frictional factor indicates the trend of smooth pipe. The data for tubes in Fig. 6 - (a), (b) also show the similar results. Unknown effects in turbulent capillary flow are considered to exist to damp the roughness effect.

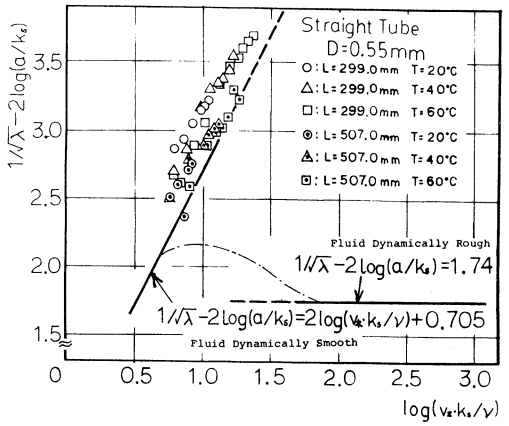

Fig. 8 Fluid dynamical roughness and friction factor in 0.55mm tube in turbulent region

As the Knudsen number (molecular mean free path)/(representative scale) seems to be small enough, molecular kinetic effect is hardly considered. Absolute scale (or time) effect may possibly exist not to develope the flow disturbance from roughness in such a fast capillary flow.

As regards the 0.29mm and 0.11mm tubes, flow characteristics are presented in Fig. 9 - (a), (b), (c). Remarkable features appear in Fig. 9 - (a), where temperature increase in water causes the transition point in pressure to shift to lower values, because of the change in kinematic viscosity. Owing to this shift, low temperature water of 20°C presents higher laminar flow rate than 60°C water in almost turbulence above 600kPa. Figure 9 -

(c) indicates the flow rates of 0.115mm straight and coiled tubes. As expected, secondary flow effect in coil yields lower discharged rate. From Fig. 9 friction factors are obtained as in Fig. 10-(a), (b), (c), which correspond well to normal tube results.

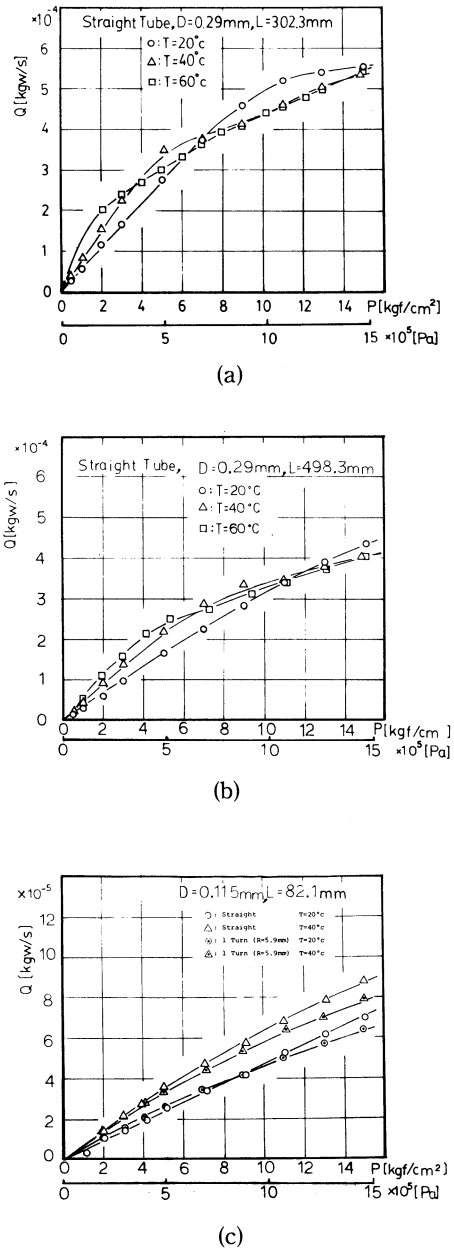

Fig. 9 Flow rates for 0.29mm and 0.115 mm tubes

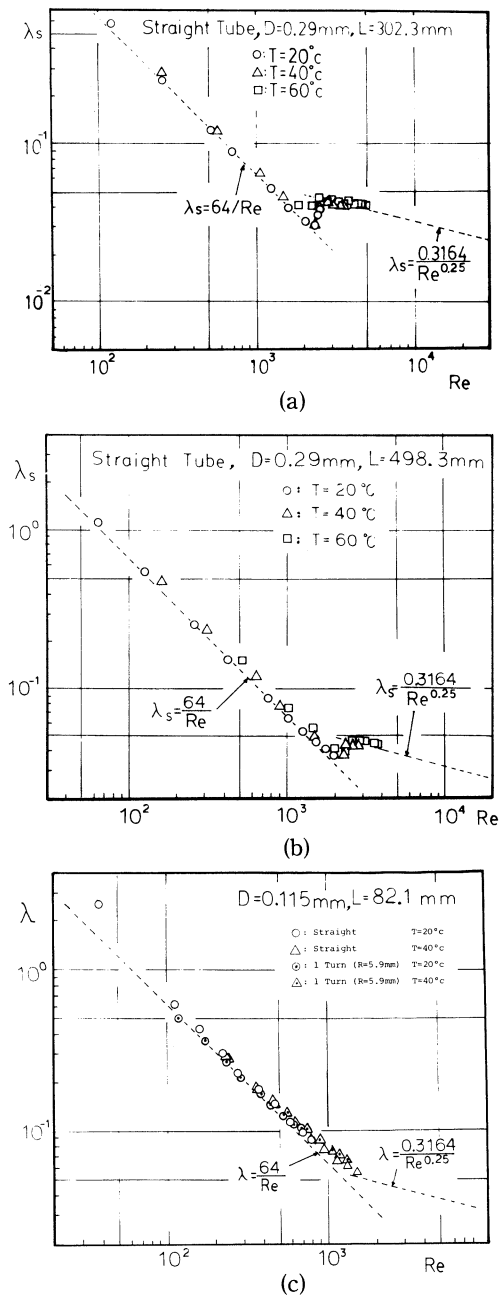

Fig. 10 Friction factor for 0.29mm and 0.115mm tubes

3-2. Bend Tube

Figures 11 - (a), (b) show the flow characteristics for tubes with 45° bend, and Fig. 12 - (a), (b), (c) for tubes with 90° bend portion. From these figures the influence of secondary flow in bend is observed mainly in laminar and transient ranges. The difference of flow rates with water temperature originates from the variation of friction factor with increased Reynolds number.

Since the Reynolds number range of 0.55mm bend is almost turbulent, total loss coefficient can be illustrated with respect to turbulent characteristic number discussed in section 2-4, as indicated in Fig. 13 - (a), (b). Dashed line represents Eq. (16) by Itō[5] and dotted marks are regarded as in transient region. Solid line shows our empirical relation obtained by least square method.

In the case of 0.29mm tube bend, both laminar and turbulent flows are realized. Then as shown in Fig. 14 - (a), (b), (c), (d), loss coefficients in laminar region can be arranged against Dean number $Re(a/R)^{1/2}$ and in turbulent flow they are placed in order by characteristic number $Re(a/R)^2$. The distributions of loss coefficient for laminar bend flow can be expressed in a single line as indicated in Fig. 14- (a), (c), which have the same trend as usual curved laminar flows. In turbulent graphs the reduced inclination of our empirical equations may be considered to be an appearance of roughness effect, but the difference from Itō's results for smooth bend are so small that we can state roughness effect in these capillaries is negligible. This peculiar result coincides with the data for straight tubes.

3-3. Coiled Capillary

As example of coiled tube, discharged flow rates for 0.29mm pipe are represented in Fig. 15 - (a), (b), (c). It is noticed that the data for straight tube clearly show the transient effect of saturation to turbulent as water temperature goes up, while the data for coiled tube still remain in laminar (or semi-laminar) keeping high flow rates. With these discharged characteristics, estimated friction factors for coiled tube of 1, 3, 6 turns are indicated in Fig. 16 - (a), (b). From these figures the range of coiled effect seems to be restricted in mainly within laminar and transient flows.[1), 2)]

According to the procedure in section 2-4, friction factors for coiled capillary are arranged. Figure 17 - (a), (b), and Fig. 18 indicate these factors multiplied by $(R/a)^{1/2}$ versus Dean number in laminar region. It can be remarked that secondary flow effect prevails over the temperature influence, and that arranged data present linear trends in logarithmic coordinates. And especially our data clearly indicate a dependence on turning angle (coiling number) as in Fig. 17 - (a), (b). As the number of coiling increases, absolute value of inclination of group data becomes smaller.

In the discussion in section 2-4, Equation (18) or (19) includes no effect of turning angle, which offers no explanation for the peculiar tendency. In our measurement, for example, the flow in 0.55mm coil of one turn with Dean number 6×10^2 has the high Reynolds number

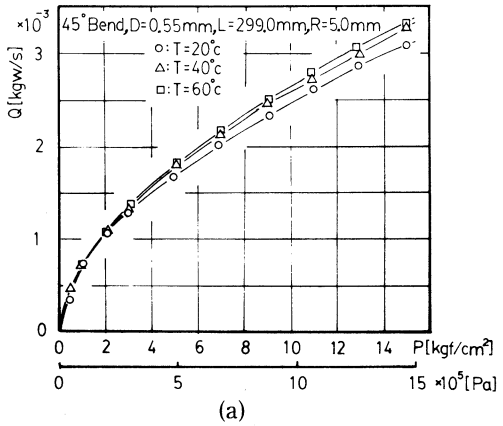

(a)

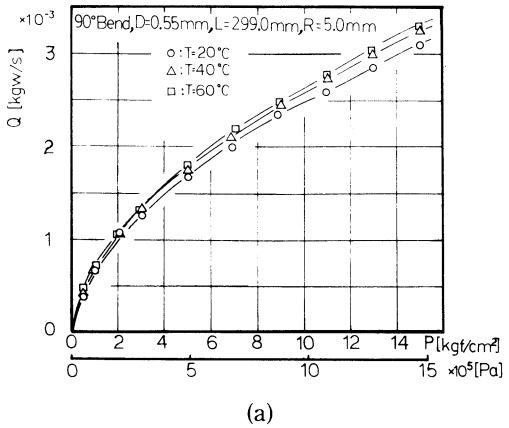

(a)

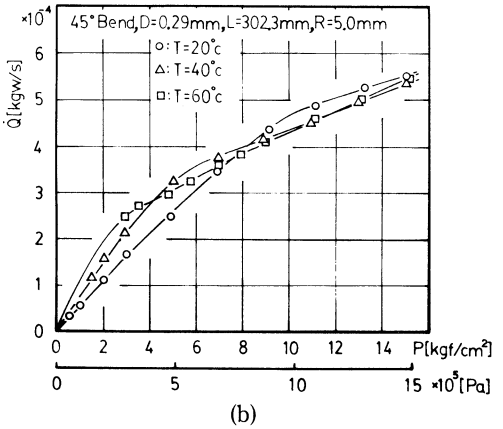

(b)

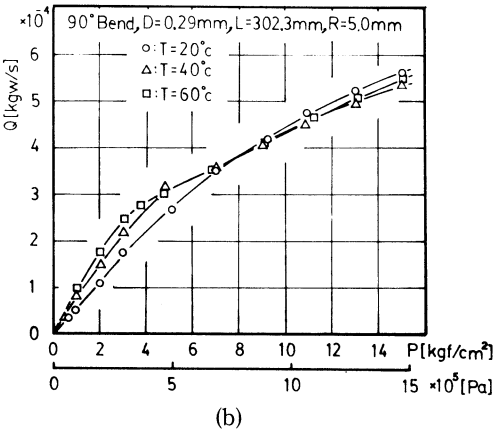

(b)

Fig. 11 Flow characteristics for tubes with 45° bend

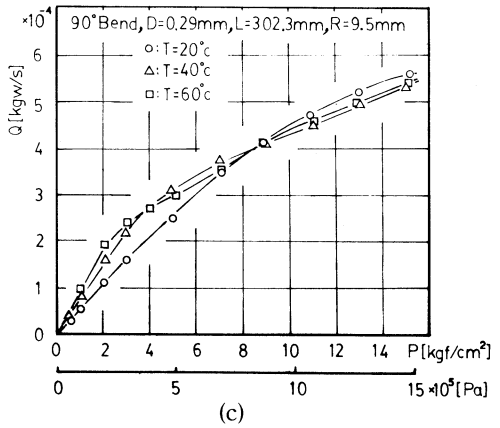

(c)

Fig. 12 Flow characteristics for tubes with 90° bend

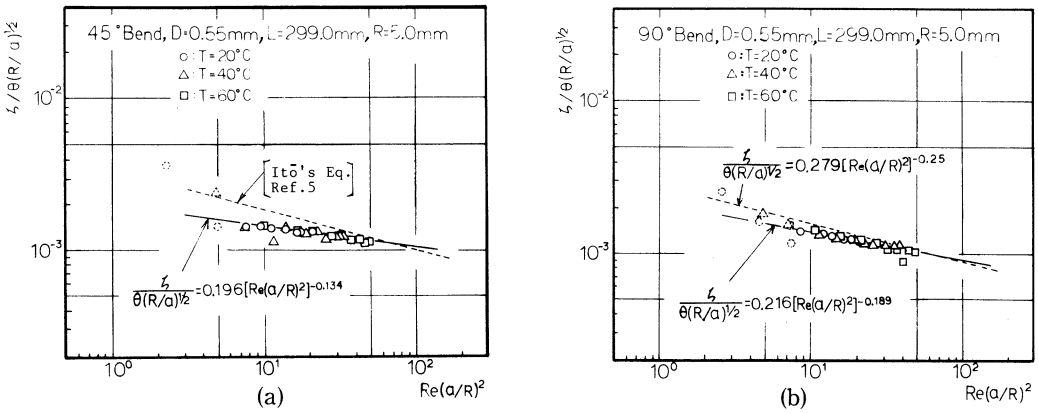

Fig. 13 Loss coefficient in turbulent bend flows vs. characteristic number for curved tube

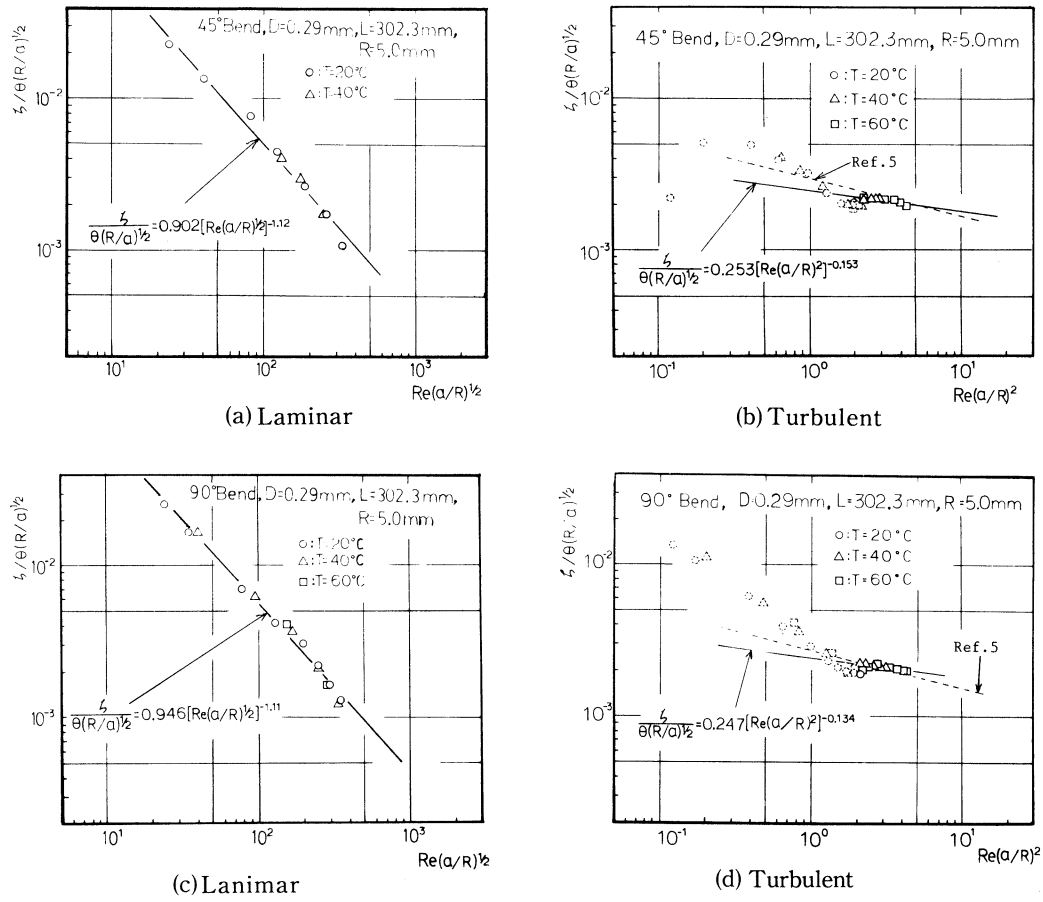

Fig. 14 Loss coefficient of 0.29mm tube bend for laminar and turbulent flows

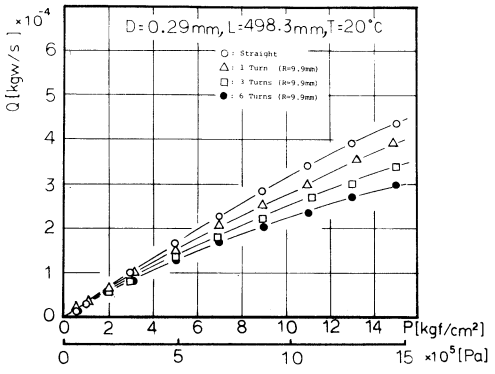

(a)

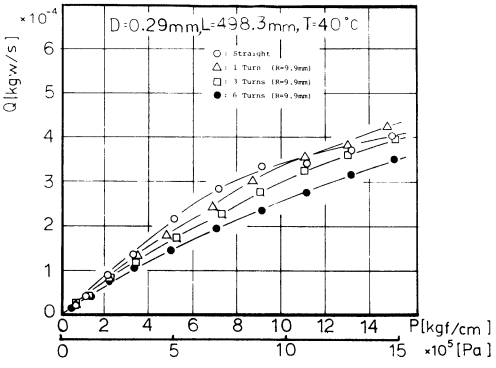

(b)

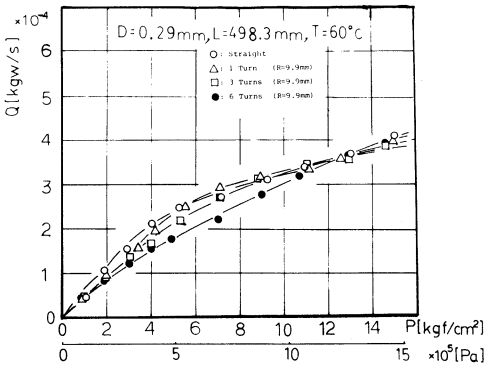

(c)

Fig. 15 Coiled effect on discharged flow rates

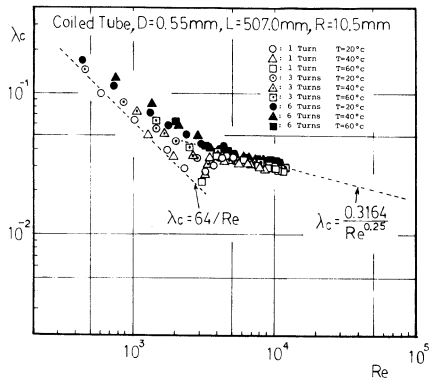

(a)

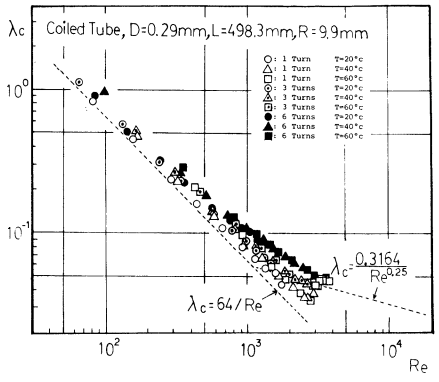

(b)

Fig. 16 Friction factor for coiled tubes

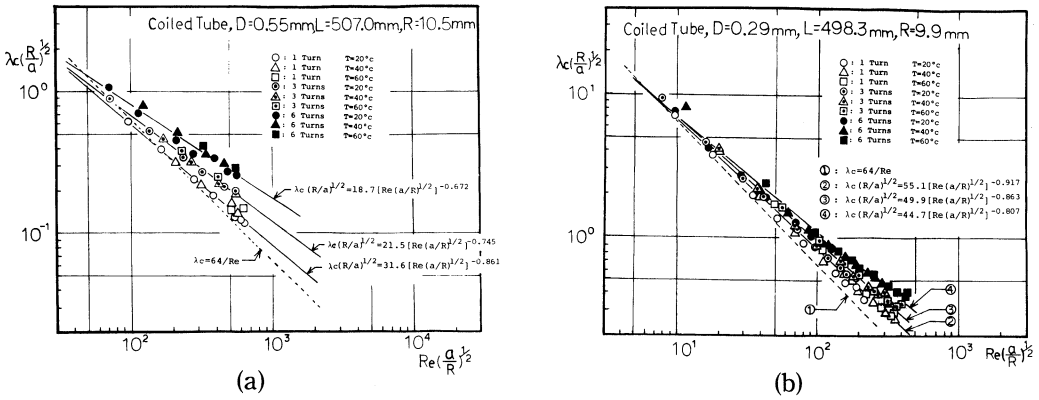

Fig. 17 Friction factor vs. Dean number for coiled tubes

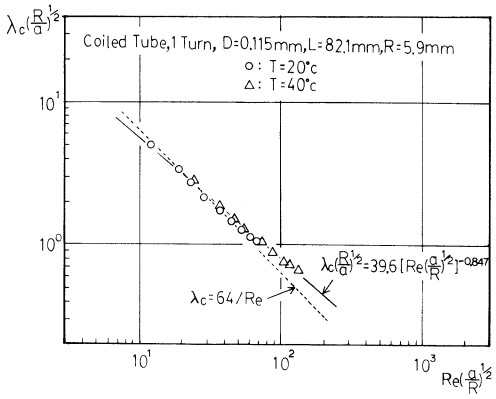

Fig. 18 Friction factor vs. Dean number for 0.115mm coil

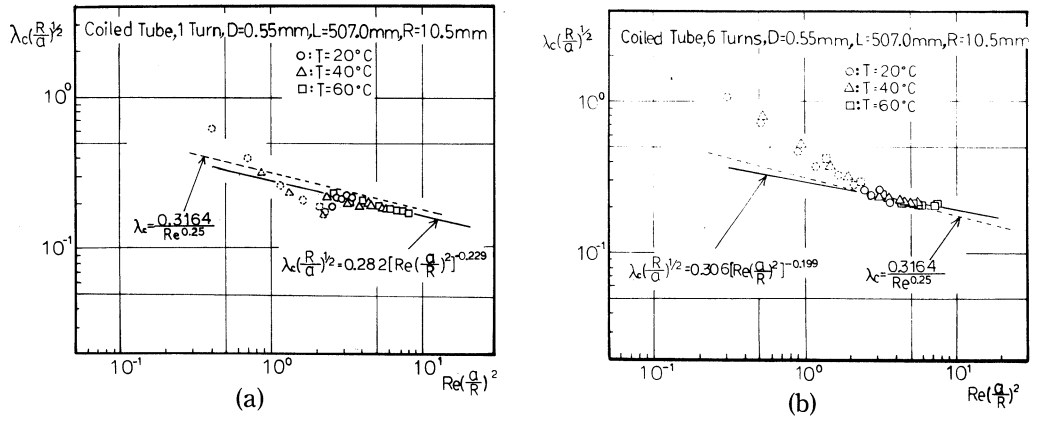

Fig. 19 Friction factor vs. turbulent chracteristic number in 0.55mm coil

of about 3.7×10^3 (transition region). Since the kinematic viscosity at 20°C is about $1.0\times10^{-6}m^2/s$, the mean flow velocity in this coil becomes up to 6.7m/s, and the value of acceleration by centrifugal force is 4.3×10^3 m/s^2 (4.4×10^2 gal). This strong acceleration seems to cause not secondary, but also the dominant circulating flow field. As the flowing duration in this coiled tube is about 70ms (at 6.7m/s), it is uncertain to establish fully developed secondary (but dominant) flow in the coil, which is considered to be one of the reasons of the trend in Fig. 17.

From the discussion above mentioned, the linear relation between $\lambda_c\,(R/a)^{1/2}$ and Dean number in logarithmic coordinates are assumed in Figs. 17 and 18. Solid lines in these figures indicate empirical equations obtained by least square method.

Figure 19 - (a), (b) show friction factor of 0.55mm coiled capillary versus turbulent characteristic number. In the graphs dotted marks are seemed to be laminar or transient. In turbulent region, measured data indicate less dependence on coiling number than in laminar and transient flow, and they do not deviate largely from Blasius' relation, as was presented in the data for bend capillary. Solid line indicates experimental equation by the method mentioned above. The measured turbulent data in these coil also do not exhibit roughness effect.

4. CONCLUSION

From the study mentioned above, following points are concluded. By the microscopic photograph of tube cross sections, equivalent diameters are measured and relatively high roughnesses are observed, where relative roughnesses of 0.55mm, 0.29mm, and 0.115mm tube are 2.5%, 4%, and 7.8%, respectively. In spite of these considerable roughnesses, measured data for straight, bent, and coiled capillaries do not indicate roughness effect explicitly. Measured flow rates show temperature dependency originated fron transition to turbulent flow with decreased kinematic viscosity.

Frictional loss of capillary bend in laminar and turbulent regions presents presumed tendency for curved pipe. Empirical equations for loss coefficient can be obtained to compare with previous investigations (turblent bend).[5] Coefficients obtained are summarized in Table 6.

Friction factors for coiled capillary in laminar range show secondary flow effect as expected. The trends obtained, however, indicate the dependence on coiling number, which cannot be explained by previous studies. Empirical equations for coiled capillary are found and compared with Itō's results, as shown in Table 7.

ACKNOWLEDGMENT

The authors are grateful to express their sincere thanks to Prof. K. Tagashira and Mr. Y. Nosaku of Muroran Institute of Technology for their great help for taking microscopic photographs of tube cross section, and also to Dr. H. Suzuki of Ishikawajima-Harima

Heavy Industries Co. Ltd. for his valuable discussion.

Table 6 Empirical equations for loss coefficient in capillary bend

(1) Laminar Flow

$$\zeta/[\theta(R/a)^{1/2}] = A\cdot Re(a/R)^{1/2}]^B$$

D	L	R	θ	Experimental	
				A	B
0.29	302.3	5	45	0.902	−1.12
0.29	302.3	5	90	0.946	−1.11
0.29	302.3	9.5	90	0.671	−1.03

(2) Turbulent Flow

$$\zeta/[\theta(R/a)^{1/2}] = A\cdot[Re(a/R)^2]^B$$

D	L	R	θ	Experimental		Itō's Equation	
				A	B	A	B
0.55	299.0	5	45	0.196	−0.134	0.331	−0.25
0.55	299.0	5	90	0.216	−0.189	0.279	
0.29	302.3	5	45	0.253	−0.153	0.298	
0.29	302.3	5	90	0.247	−0.134	0.276	
0.29	302.3	9.5	90	0.289	−0.150	0.276	

Table 7 Empirical equations for friction factor in coiled capillary

(1) Laminar Flow

$$\lambda_C(R/a)^{1/2} = A\cdot[Re(a/R)^{1/2}]^B$$

D	L	R	N	θ	Experimental		Darcy	
					A	B	A	B
0.55	507.0	10.5	1	360	31.6	−0.861	64	−1
0.55	507.0	10.5	3	1080	21.5	−0.745		
0.55	507.0	10.5	6	2160	18.7	−0.672		
0.29	498.3	6.2	1	360	61.6	−0.964		
0.29	498.3	6.2	3	1080	45.8	−0.878		
0.29	498.3	6.2	6	2160	37.4	−0.806		
0.29	498.3	9.9	1	360	55.1	−0.917		
0.29	498.3	9.9	3	1080	49.9	−0.863		
0.29	498.3	9.9	6	2160	44.7	−0.807		
0.115	82.1	5.9	1	360	39.6	−0.847		

(2) Turbulent Flow

$$\lambda_C(R/a)^{1/2} = A\cdot[Re(a/R)^2]^B$$

D	L	R	N	θ	Experimental		Darcy	
					A	B	A	B
0.55	507.0	10.5	1	360	0.282	−0.229	0.3164	−0.25
0.55	507.0	10.5	3	1080	0.270	−0.191		
0.55	507.0	10.5	6	2160	0.306	−0.199		

REFERENCES

1) H. Schlichting ; "Boundary-Layer Theory," 7th Ed., McGraw-Hill (1979).

2) R. P. Benedict ; "Fundamentals of Pipe Flow," John Wiley & Sons (1980).

3) W. R. Dean ; "Note on the Motion of Fluid in a Curved Pipe," Philosophical Magazine, S. 7, Vol. 4, No. 20 (1927), pp. 208-223.

4) W. R. Dean ; "The Stream-line Motion of Fluid in a Curved Pipe," Philosophical Magazine, S. 7, Vol. 5, No. 30 (1928), pp. 673-695.

5) H. Itō ; "Pressure Losses in Smooth Pipe Bends," Transactions of the ASME, J. of Basic Engng., Vol. 82, No. 1 (1960), pp. 131-143.

6) S. Zafran, C. K. Murch, and R. Grabbi ; "Flight Applications of High Performance Electrothermal Thrusters," AIAA Paper, No. 77-965 (1977).

7) F. X. McKevitt ; "Design and Development Approach for The Augmented Catalytic Thruster (ACT)," AIAA Paper, No. 83-1255 (1983).

8) S. T. McComas ; "Hydrodynamic Entrance Lengths for Ducts of Arbitrary Cross Section," Transactions of the ASME, J. of Basic Engng., Vol. 89, No. 4 (1967), pp. 847-850.

9) D. A. Bowlus and J. A. Brighton ; "Incompressible Turbulent Flow in the Inlet Region of a Pipe," Transactions of the ASME, J. of Basic Engng., Vol. 90, No. 3 (1968), pp. 431-433.

10) H. Itō ; "Flow and Loss in Curved Tubes, (in Japanese)," Journal of the JSME, Vol. 62, No. 490 (1959), pp. 1634-1643.

11) H. Itō ; "Laminar Flow in Curved Pipes," ZAMM, Bd. 49, Heft 11 (1969), pp. 653-663.

12) H. Itō ; "Friction Factors for Turbulent Flow in Curved Pipes," Transactions of the ASME, J. of Basic Engng., Vol. 81, No. 2 (1959), pp. 123-134.